JOURNAL OF THE AMERICAN CHEMICAL SOCIETY

Article

Highly Stable Zr(IV)-Based Metal-Organic Frameworks for the Detection and Removal of Antibiotics and Organic Explosives in Water

Bin Wang, Xiu-Liang Lv, Dawei Feng, Lin-Hua Xie, Jian Zhang, Ming Li, Yabo Xie, Jian-Rong Li, and Hong-Cai Zhou

J. Am. Chem. Soc., **Just Accepted Manuscript** • DOI: 10.1021/jacs.6b01663 • Publication Date (Web): 19 Apr 2016

ACS Publications

Journal of the American Chemical Society is published by the American Chemical Society. 1155 Sixteenth Street N.W., Washington, DC 20036

Highly Stable Zr(IV)-Based Metal-Organic Frameworks for the Detection and Removal of Antibiotics and Organic Explosives in Water

Bin Wang,[†] Xiu-Liang Lv,[†] Dawei Feng,[‡] Lin-Hua Xie,[†] Jian Zhang,[†,§] Ming Li,[§] Yabo Xie,[†] Jian-Rong Li,[*,†] and Hong-Cai Zhou[‡]

[†] Beijing Key Laboratory for Green Catalysis and Separation and Department of Chemistry and Chemical Engineering, College of Environmental and Energy Engineering, Beijing University of Technology, Beijing 100124, P. R. China

[‡] Department of Chemistry, Texas A&M University, College Station, TX 77843, USA

[§] State Key Laboratory Base of Eco-Chemical Engineering, College of Chemistry and Molecular Engineering, Qingdao University of Science and Technology, Qingdao 266042, P. R. China

KEYWORDS: Antibiotic, Organic Explosive, Metal-Organic Framework, Selective Detection, Adsorption

ABSTRACT: Antibiotics and organic explosives are among the main organic pollutants in wastewater; their detection and removal are quite important but challenging. As a new class of porous materials, metal-organic frameworks (MOFs) are considered as promising platform for the sensing and adsorption applications. In this work, guided by a topological design approach, two stable isostructural Zr(IV)-based MOFs, $Zr_6O_4(OH)_8(H_2O)_4(CTTA)_{8/3}$ (BUT-12, H_3CTTA = 5′-(4-carboxyphenyl)-2′,4′,6′-trimethyl-[1,1′:3′,1′′-terphenyl]-4,4′′-dicarboxylic acid) and $Zr_6O_4(OH)_8(H_2O)_4(TTNA)_{8/3}$ (BUT-13, H_3TTNA = 6,6′,6′′-(2,4,6-trimethylbenzene-1,3,5-triyl)tris(2-naphthoic acid)) with the **the-a** topological structure constructed by D_{4h} 8-connected Zr_6 clusters and D_{3h} 3-connected linkers were designed and synthesized. The two MOFs are highly porous with the BET surface area of 3387 and 3948 m^2 g^{-1}, respectively. Particularly, BUT-13 features one of the most porous water-stable MOFs reported so far. Interestingly, these MOFs represent excellent fluorescent properties, which can be efficiently quenched by trace amounts of nitrofurazone (NZF) and nitrofurantoin (NFT) antibiotics, as well as 2,4,6-trinitrophenol (TNP) and 4-nitrophenol (4-NP) organic explosives in water solution. They are responsive to NZF and TNP at parts per billion (ppb) levels, which are among the best performing luminescent MOF-based sensing materials. Simultaneously, both MOFs also display high adsorption abilities towards these organic molecules. It was demonstrated that the adsorption plays an important role in the pre-concentration of analytes, which can further increase the fluorescent quenching efficiency. These results indicate that BUT-12 and -13 are favorable materials for the simultaneous selective detection and removal of specific antibiotics and organic explosives from water, being potentially useful in monitoring water quality and treating wastewater.

Introduction

With ever-increasing concern for public health and water quality, there is now a much greater demand for the detection and removal of pollutants from wastewater. Antibiotics being used extensively for the treatment of bacterial infections in humans and animals have been noticed as a class of important organic pollutes in water. The abuse of antibiotics has led to high level of antibiotic residues. Various antibiotics have been detected in both surface and ground water, as well as even in drinking water. Recent research shows that the total antibiotic usage in China in 2013 was approximately 162000 tons, and this number was further increasing with the development of the industry and the increase of the populations.[1,2] Similarly, nitroaromatics widely used as explosives are also undesirable organic pollutions in wastewater apart from antibiotics. These chemicals are highly poisonous and difficult to be degraded by nature. Monitoring and removing these specific pollutants from water are quite important, but challenging. Till now, the detection of antibiotics and nitroaromatics is mainly based on instrumental methods such as liquid chromatography-tandem mass spectrometry (LC-MS),[3] LC with UV detection (LC-UV),[4] capillary electrophoresis (CE),[5] mass spectrometry (MS),[6] raman spectroscopy (RS),[7] and ion mobility spectrometry (IMS).[8] However, all these methods are time-consuming, expensive, and require complex equipment and trained personnel. In addition, technologies for the removal of antibiotics are not so mature yet, although a variety of methods including photolysis,[9] hydrolysis, and thermolysis,[10] technical oxidation processes,[11] as well as biodegradation[12] have been developed, which are all based on chemical treatment. Therefore, the development of portable, reliable, and inexpensive methods/technologies for the detection and removal of antibiotics and nitroaromatics pollutants have been a matter of great concern to researchers.

Alternately, optical sensing[13] and adsorption based methods[14] have been considered as promising technologies in the detection and removal of antibiotics and organic explosives, respectively, because of some advantages, such as easy operation, energy-saving, high efficiency, and so on. Although some progresses have been made in this regards, great efforts are still required to put the application into practice. The challenge of developing these methods rests with the selection of materials, which should incisively respond to the checked molecules. Up to now, a lot of checked materials display only one function as either the sensing materials or the adsorbent. Integrating these two functions into one material is clearly favorable, but rarely identified. Using such a multifunctional material would be not only cost effective but also efficiency improved. Besides, the adsorption process can allow the pre-concentration of target analytes, thus increasing the detection ability of the material.[15-17]

Porous materials are promising candidates for integrating these two functions. However, because of the difficulty in the modification of the pores, the application of traditional porous materials, such as activated carbon, zeolites, aluminosilicates, etc. is limited to some extent. As a class of newly developed porous solids, metal-organic frameworks (MOFs), constructed by metal ions or metal clusters and organic ligands through coordination bonds, are considered as favorable platform for the detection/sensing[18-22] and adsorption[23,24] applications because of their specific electronic and optical properties, permanent porosity, high surface area, and easily tailorable structures and functions. Particularly, through ligand modifications, various fluorophores can be rationally introduced into the pores of MOFs, which makes them show excellent fluorescent property without loss of porosities.[25] As a result, the simultaneous detection and removal of specific chemical species using MOFs become possible and accessible.

Some MOFs have been explored for the detection of explosives and shown excellent detection abilities and selectivities.[18-20] However, most of them were checked in organic solvents instead of water. And, to the best of our knowledge, there is no report in using MOFs as sensing materials to detect antibiotics. Moreover, documented publications concerning aqueous-phase adsorption and removal of organic contaminants using MOFs are limited to benzene,[26] organic dyes,[27] pharmaceuticals,[28] phenol, bisphenol A,[29] 2,4-dichlorophenoxyacetic acid,[30] and *p*-cresol.[31] Very few works have been reported in the removal of antibiotics and explosives by using MOFs as adsorbents.[32,33]

In addition, for the applications of MOFs in water system, such as the pollutants detection and removal mentioned herein, the water stability of their frameworks is of the precondition.[34,35] Unfortunately, a large number of reported MOFs are not stable in water, except for some examples of ZIFs, MILs, CAUs, UiOs and other Zr(IV)-based MOFs, and so on.[36,37] Generally, there are two ways to improve the water stability of carboxylate-based MOFs: (1) incorporating hydrophobic groups near coordination sites or onto linkers through direct synthesis or postsynthetic modification to enhance the hydrophobic property of MOFs, thereby protecting coordination bonds from hydrolysis[38-44] and (2) using high oxidation state metals (such as Cr^{3+}, Fe^{3+}, Al^{3+}, and Zr^{4+}) to form strong coordination bonds with organic carboxylate ligands.[45-48]

In this work, guided by a topological design approach, two isostructural Zr-MOFs, $Zr_6O_4(OH)_8(H_2O)_4(CTTA)_{8/3}$ (BUT-12, where BUT = Beijing University of Technology) and $Zr_6O_4(OH)_8(H_2O)_4(TTNA)_{8/3}$ (BUT-13) were designed and synthesized through the reaction of $ZrCl_4$ with two pre-designed fluorescent ligand acids, 5′-(4-carboxyphenyl)-2′,4′,6′-trimethyl-[1,1′:3′,1′′-terphenyl]-4,4′′-dicarboxylic acid (H_3CTTA) and 6,6′,6′′-(2,4,6-trimethylbenzene-1,3,5-triyl)tris(2-naphthoic acid) (H_3TTNA), respectively. The framework structures of the two MOFs exhibit the **the-a** topology with D_{4h} 8-connected Zr_6 cluster nodes and D_{3h} 3-connected ligand linkers. Both MOFs show high surface area and moderate pore sizes, as well as good stability in water, HCl solutions (2 M, 6 M, and concentrated HCl), and NaOH solutions (pH = 10). Particularly, they represent excellent fluorescent property. Based on their outstanding water stability, porosity, and fluorescence, the detection and removal of selected antibiotics and nitroaromatics were explored in the two MOFs. Twelve antibiotics of five classes: nitrofurans (NFs), nitroimidazole (NMs), sulfonamides (SAs), chloramphenicols (CPs), and β-lactams, and eleven nitroaromatics were studied. It has been found that both BUT-12 and -13 represent high fluorescence quenching efficiency and high adsorption ability towards nitrofurazone (NZF) and nitrofurantoin (NFT) antibiotics and 2,4,6-trinitrophenol (TNP) and 4-nitrophenol (4-NP) nitroaromatics. The detection limits of BUT-12 towards NZF and TNP are estimated to be 58 and 23 ppb, and those of BUT-13 are 90 and 10 ppb, respectively. It has also been demonstrated that the adsorption process indeed plays an important role in the enrichment of NFs, TNP, and 4-NP, which further increase the quenching efficiency of the MOFs.

Results and discussion

Design and synthesis

Zr-MOFs have been extensively studied since the development of using modulating reagents to assist single crystals production.[49,50] However, compared with a lot of other metal species which can form many different clusters with various symmetries and connectivities, the overwhelming majority of Zr-MOFs are based on Zr_6 carboxylate cluster, which severely limits their topology diversity, and thus requires judicious design of the overall MOF structures rather than simply varying the symmetry and connectivity of used ligands. Try-error could thus easily lead to amorphous products due to the topological incompatibility between the organic linkers and the Zr_6 cluster. On the other hand, even though crystalline product can be obtained, lack of large crystals suitable for single crystal characterization still hinders the development of Zr-MOFs with new structures. Therefore, the design of Zr-MOFs with targeting structures is of great importance.

As aforementioned, Zr_6 cluster is the dominant secondary building unit (SBU) core in Zr-MOFs. Despite of this, the high symmetry and connectivity enable Zr_6 cluster serving as different types of nodes in the resulting networks via reducing the connectivity, making it compatible to form three dimensional (3D) periodic frameworks with different linkers. As such, the possible symmetry and connectivity of Zr_6 cluster can be easily predicted. Since many binodal networks have been presented,[51] one of the most convenient approaches to construct a new Zr-MOF is to fit Zr_6 cluster with compatible symmetry and connectivity as one node into a binodal network, and then design specific organic linkers as the compatible counter-parts.[52]

So far, Zr_6 clusters with several connectivities have been reported, including twelve,[47,53,54] ten,[54,55] eight,[52,54,56-59] and six.[54,60,61] Among them, D_{4h} 8-connected node is able to form several binodal networks with different linkers, such as **scu-a**, **flu-a**, **ocu-a**, and **the-a** networks (Figure 1a).[51] However, only **flu-a** network has been realized in Zr-MOFs among those four.[52,54,59] For the **ocu-a** network, it is challenging because D_{3d} 6-connected linker is required, which is not common for organic linkers. While the **scu-a** and **the-a** networks are supposed to be more feasible owing to the ease of their organic linker synthesis. In the former, a D_{4h} or D_{2h} 4-connected linker

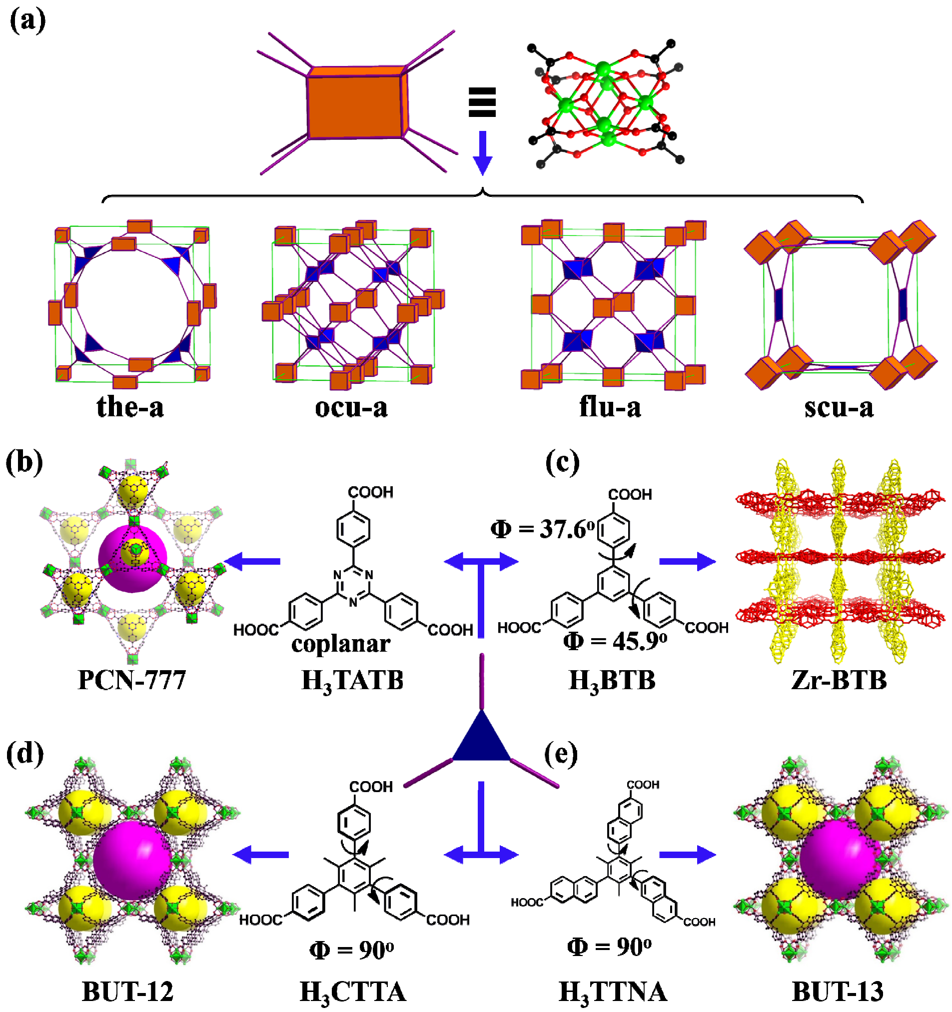

Figure 1. (a) Topological analysis of binodal edge-transitive networks with D_{4h} 8-connected Zr_6 clusters and different linkers; (b) structures of H_3TATB and PCN-777; (c) structures of H_3BTB and Zr-BTB; (d) structures H_3CTTA and BUT-12; and (e) structures of H_3TTNA and BUT-13 (Color code: C, black; O, red; and Zr, green; H atoms on ligands are omitted for clarity; the large pink and yellow spheres represent cage void regions inside the frameworks).

is required and in the latter it is a D_{3h} 3-connected linker. Nevertheless, 4-connected D_{4h} and D_{2h} linkers are also compatible with many other Zr_6 nodes, when the energy of the linker and overall connectivity of the framework are taken into account, **scu-a** network may not be the thermodynamically favored outcome. Consequently, the **scu-a** network is missing in Zr-MOFs.

In comparison, a D_{3h} 3-connected linker required in the **the-a** network is one type of the most frequently adopted linkers in MOFs. However, although three Zr-MOFs constructed with 3-connected linkers have been reported, namely MOF-808,[54] PCN-777,[60] and Zr-BTB,[61] a **the-a** type Zr-MOF is still missing. Actually, when the entropy effect is considered, the **the-a** network is more thermodynamically favored because of its higher connectivity compared to those three MOFs. Therefore, it is puzzling that the **the-a** type Zr-MOF has not been synthesized yet with benzene-1,3,5-tricarboxylate (BTC^{3-}), 4,4′,4′′-*s*-triazine-2,4,6-triyltribenzoate ($TATB^{3-}$), and 1,3,5-benzenetribenzoate (BTB^{3-}) ligands, which suggests there might be some key point missed in a traditional topology guided design of the MOFs.

In a typical topological simplification of a MOF, only the connectivity and symmetry of each node in the network are considered. After the simplification, the connection between different nodes is always represented by a line without other details, such as the direction preference of the coordination bond. However, in a reverse way when topological analysis is used as a tool to design MOFs, these details have to be considered to avoid the high energy configuration of either the inorganic cluster or the organic linker. Otherwise, the resulting product will quite possibly be thermodynamically unfavored.[53] In the **the-a** network, when the D_{4h} Zr_6 cluster is placed in the position of the 8-connected node, it fits perfect in terms of the connectivity and symmetry. However, if we take a close look at the orientation of three carboxylates on three neighboring Zr_6 clusters, which are supposed to be connected by a D_{3h} node, they do not stay in the same plane. Instead, those three carboxylates are perpendicular to the same plane, which suggests that the D_{3h} 3-connected linker has to adopt the same configuration in order to fit the network. Whereas, in BTC^{3-} and $TATB^{3-}$, three carboxylate groups prefer to be coplanar due to their large conjugation system (Figure 1b). In BTB^{3-}, although the perfect coplanar configuration of three carboxylates is not the favorite, the energy of the ligand is much higher when three carboxylates are perpendicular to the central phenyl ring (Figure 1c). Therefore, none of these three ligands prefer to stay in the **the-a** network with D_{4h} 8-connected Zr_6 cluster. To overcome the conflict between topological preference and ligand configuration preference, a D_{3h} 3-connected ligand, which allows three carboxylates to stay perpendicularly to the same plane, is necessary.

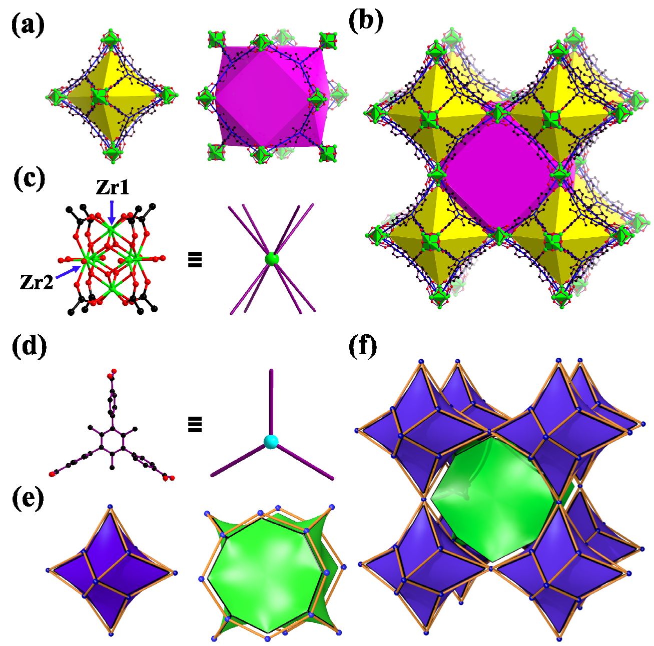

Figure 2. (a, b) Polyhedral cages and their 3D packing in BUT-12; (c, d) view of the $[Zr_6O_4(OH)_8(H_2O)_4(COO)_8]$ SBU node and $CTTA^{3-}$ ligand in BUT-12, respectively, (e, f) the natural tiling of polyhedral cages in BUT-12. (Color code: C, black; O, red; and Zr, green; H atoms on ligands are omitted for clarity).

Hence, we designed and synthesized two carboxylate ligands preferring such a configuration, $CTTA^{3-}$ and $TTNA^{3-}$. The former is a derivative of BTB^{3-}. Differently, the central phenyl ring is functionalized with three methyl groups, which can force three peripheral phenyl rings perpendicular to the central one because of the steric hindrance, while still gives rise to the D_{3h} symmetry. Besides, the presence of three methyl groups on the central phenyl ring of the ligands can increase the hydrophobicity of the framework, therefore probably leading to a further enhanced water stability of resulting Zr-MOF. On the other hand, fixing the terminal phenyl rings to a rigid structure can efficiently eliminate non-radiative relaxation pathways, thus increase the fluorescent property of itself as well as derived MOFs.[62-64] In addition, naphthalene ring is recognized as a good fluorescent group, thus the replacement of phenyl rings in $CTTA^{3-}$ with naphthalene rings will further improve the luminescent property of resulting MOF with $TTNA^{3-}$ (Figure 1d and e). As a result, the lowest energetic configuration of $CTTA^{3-}$ and $TTNA^{3-}$ matches the symmetry and orientation requirement in the **the-a** network, making it thermodynamically preferred product.

As we expected, solvothermal reactions of H_3CTTA or H_3TTNA with $ZrCl_4$ in the presence of formic acid or acetic acid as competing reagents in DMF yielded cubic-shaped single crystals of BUT-12 and -13, respectively. In the synthesis of Zr-MOFs, it has been confirmed that additional acid modulators play an important role in controlling the nucleation rate of forming products.[49] Without modulators, the Zr-MOFs precipitate as micro-sized aggregates of nanocrystals or disordered phases were usually obtained. In our case, formic acid or acetic acid was used as the modular reagent to obtain pure crystalline samples of BUT-12 and -13, which were confirmed by powder X-ray diffraction (PXRD) (Figure 3a and b). After precisely tuning the amounts of the modulators, single crystals big enough for the single-crystal X-ray diffraction were finally obtained. In addition, in the FT-IR spectra of BUT-12 and -13, slight blue shifts of carbonyl group characteristic bands compared with corresponding ligands were observed, illustrating the metal coordination of carboxylate groups in these ligands (Figure S4 in the Supporting Information).

Structural description

Single-crystal X-ray diffraction reveals that BUT-12 crystallizes in the cubic space group *Pm*–3*m* with the lattice parameter a = 28.199 (7) Å (Table S1 in the Supporting Information). In the structure, there exist two crystallographically independent Zr atoms (Zr1 and Zr2), which are all eight-coordinated in a tetragonal antidipyramid coordination geometry (Figure 2c). Zr1 is coordinated by four O atoms from different carboxylate groups and four μ_3-OH/O moieties, while Zr2 is coordinated by two O atoms from different carboxylate groups, four μ_3-OH/O moieties, and two terminal –OH/H_2O entities. Six Zr atoms connected with each other by four μ_3-O and four μ_3-OH groups to form a $Zr_6O_4(OH)_4$ core. The core can be described as a Zr_6 octahedron, in which the vertices are occupied by Zr atoms and the faces are capped by eight μ_3-OH/O atoms. Furthermore, eight of the twelve octahedral edges are connected to CTTA^{3-} ligands through the carboxylate coordination, while the remaining Zr coordination sites are occupied by eight terminal –OH/H_2O groups to form a $[Zr_6O_4(OH)_8(H_2O)_4(CO_2)_8]$ SBU (Figure 2c). The same SBU was also observed in NU-1000[56] and PCN-222.[57] These SBUs are linked by CTTA^{3-} ligands to form a 3D framework with two types of polyhedral cages. One is octahedral, with six Zr(IV)-based SBUs occupying the vertices and eight CTTA^{3-} linkers covering the faces (Figure 2a). The size across the edge of an octahedral cage is about 17.5 Å (atom to atom distance). The other one is a cuboctahedral cage constructed by twelve SBUs and eight CTTA^{3-} ligands. This cage consists eight triangular and six square faces and can enclose a sphere of diameter 24.7 Å (atom to atom distance) inside its pore (Figure 2a). In the structure, one cuboctahedral cage is joined to six other cuboctahedral cages through sharing square windows and to eight octahedral cages through sharing triangular windows to finish the whole framework construction. From the topological view point, the Zr_6 cluster serves as a 8-connected node (Figure 2c) and the CTTA^{3-} ligand can be seen as a 3-connected node (Figure 2d), the 3D structure of BUT-12 can thus be simplified as a 3,8-c binodal net with the point symbol of $\{4^3\}8\{4^8.6^4.8^{12}.10^4\}_3$, which corresponds to the **the-a** topology, being first example among Zr-MOFs (Figure 2f).[65-67] For BUT-13, due to its high porosity, it is hard to collect a well enough diffraction data set to solve its structure through single-crystal X-Ray diffraction notwithstanding obtained single

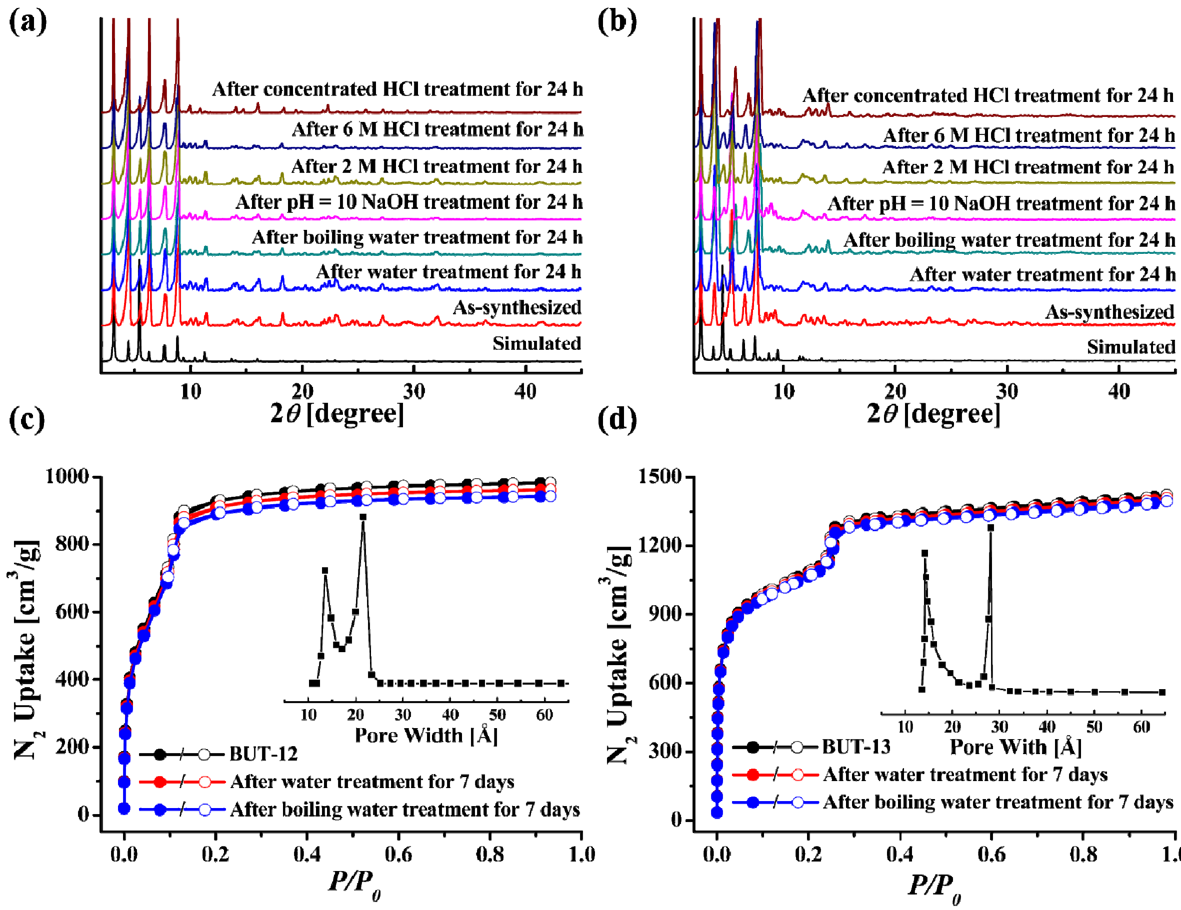

Figure 3. (a, b) PXRD patterns of BUT-12 and -13, respectively upon the treatment with water, boiling water, pH = 10 NaOH solution, 2 M HCl, 6 M HCl, and concentrated HCl; (c, d) N_2 adsorption isotherms of BUT-12 and -13 after treated in water, respectively at 77 K (Inset shows DFT pore size distribution for the corresponding MOF evaluated by using N_2 adsorption data measured at 77 K, respectively).

crystals are large (Figure S2 in the Supporting Information). We thus constructed its structure by following a reverse topological approach based on combining the computational construction method and experimental single-crystal X-Ray diffraction.[68] The detailed construction is illustrated in Figure S1 of the Supporting Information. The generated BUT-13 shares the same structure as BUT-12 and has a crystal lattice parameter of 33.223(2) Å. The size across the edge of an octahedral cage and the internal pore diameter of the cuboctahedral cage in BUT-13 are 21.3 and 30.2 Å, respectively (atom to atom distance). After removing free solvent molecules, the total solvent-accessible volumes of BUT-12 and -13 are estimated to be 79.1% and 84.6%, respectively by *PLATON*.[69]

Pore characterization

The porosities of BUT-12 and -13 were examined by N_2 adsorption at 77 K. Saturated N_2 uptakes of 982 and 1422 cm^3 g^{-1} (STP) are achieved, and evaluated Brunauer-Emmett-Teller (BET) surface areas are 3387 and 3948 m^2 g^{-1}, respectively (Figure 3c and d). The experimental total pore volumes are 1.52 and 2.20 cm^3 g^{-1} for BUT-12 and -13, being in close with the calculated values of 1.71 and 2.68 cm^3 g^{-1}, respectively. Stepwise N_2 adsorption/desorption isotherms were observed, which implies the *meso*-porosity or cage-type structure of the two MOFs.[57,70] Furthermore, we compared the pore volumes and total solvent-accessible volumes of the two MOFs with other Zr-MOFs, as well as some other water-stable MOFs (Table S2 in the Supporting Information). It was found that the pore volumes of BUT-12 and -13 are in the middle level. However, the total solvent-accessible volumes of BUT-12 are comparable or higher than other MOFs. Particularly, BUT-13 represents one of the most porous water-stable MOFs reported so far. Based on the N_2 sorption data, the pore size distributions were calculated by density functional theory (DFT) method, which gave two types of pores of 13 and 21 Å for BUT-12, and 14 and 28 Å for BUT-13 (Figure 3c and d, inset), being consistent with the crystallographic structure determination in each case when van der Waals contact is considered.

Stability test

In order to examine the chemical stability of BUT-12 and -13, the samples were checked in water, HCl solutions (2 M, 6 M, and concentrated HCl), and NaOH solution (pH = 10) at room temperature, as well as in boiling water. After being immersed in these different solutions for 24 h, the measured PXRD patterns show retained crystallinity and unchanged structures, demonstrating their excellent stability (Figure 3a and b). It should be pointed out that there are limited MOFs showing good stability in boiling water, as well as in aqueous solutions with such a wide pH range (Table S2 in the Supporting Information). As is well-known, the Zr_6 cluster is one of the most stable building units for MOF construction because the Zr^{4+} with its high charge density (Z/r) can polarize the O atoms of the carboxylate groups to form strong Zr–O bonds with significant covalent character. Besides the stable Zr_6 cluster, the excellent water stabilities of BUT-12 and -13 might also be attributed to a combination of hydrophobic effect and electronic effects of methyl groups in the ligands.[71] The methyl group is hydrophobic, which can enhance the hydrophobicity of the frameworks. On the other hand, as electron donor, methyl group can increase the electron density of both the central and the terminal benzene rings in the ligand, leading to an increase of the electron density of carboxyl O atoms, which can further increase the Zr–O bond strength. To quantitatively demonstrate such an electronic effect, DFT calculations were performed to identify the electron density of different atoms in the ligand acids by using the GAUSSIAN 03 package (for details, see Section 5 of the Supporting Information). After addition of methyl groups, the charges of O1 and O2 in the carboxyl group of H_3BTB change from −0.621 and −0.609 to −0.645 and −0.624 e in H_3CTTA, respectively. And, the charges of O1 and O2 in 6,6′,6′′-(benzene-1,3,5-triyl)tris(2-naphthoic acid) (H_3BTNA) change from −0.621 and −0.603 to −0.633 and −0.611 e in H_3TTNA, respectively (Table S3 and Figure S6 in the Supporting Information). Enhanced electron densities of carboxyl O atoms in H_3CTTA and H_3TTNA were thus justified.

In addition, as shown in Figure S3 of the Supporting Information, the thermal gravimetric analysis (TGA) curves indicate that BUT-12 and -13 are thermally stable up to 320 and 430 °C, respectively. Generally, the thermal stability of MOFs is related to the strength of the associated metal coordination bond, as well as the nature of used ligands.[72] Since the two MOFs have isoreticular structures with close Zr–O bond strength, the different thermal stability of them is probably caused by the different decomposition temperatures of the two ligands, which are related with their different structures and molecular weights.

Detection of antibiotics and nitroaromatics

Because of the high porosity and excellent water stability of BUT-12 and -13, we sought to explore their application in monitoring antibiotics and nitroaromatics in water through fluorescent sensing. The solid-state luminescent properties of H_3CTTA, H_3TTNA, BUT-12, and BUT-13 were firstly checked at room temperature. As shown in Figure S7 (see the Supporting Information), the ligand acids, H_3CTTA and H_3TTNA exhibit fluorescent emissions at 381 and 399 nm upon the excitations at 312 and 324 nm, respectively. Compared with the free H_3CTTA and H_3TTNA, BUT-12 and -13 show similar emissions at 372 and 410 nm based on the same excitations as their corresponding ligand acids, respectively, which indicates that the fluorescence of BUT-12 and -13 is mainly attributed to the emission of the organic ligands. Furthermore, the fluorescent properties of BUT-12 and -13 dispersed in different solvents were investigated (Figure S8 in the Supporting Information). It was found that the fluorescent emissions of them have slight solvent-dependence and both MOFs represent excellent fluorescent emissions in water, being promising candidates for the detection applications in water system. The highly water stability together with good fluorescent performances of BUT-12 and -13 prompt us to explore their fluorescent sensing properties in water.

To explore the ability of BUT-12 and -13 to sense a trace quantity of antibiotics, fluorescence-quenching titrations were performed with the piece by piece addition of antibiotics to water where BUT-12 and -13 are dispersed. Five classes of frequently-used antibiotics, NFs (furazolidone, FZD; nitro-furazone, NZF; nitrofurantoin, NFT), NMs (ronidazole, RDZ; metronidazole, MDZ; dimetridazole, DTZ; ornidazole, ODZ), sulfonamides (sulfadiazine, SDZ; sulfamethazine, SMZ), chloramphenicols (chloramphenicol, CAP; thiamphenicol, THI), and β-lactams (Penicillin, PCL) were checked (Figure S9 in the Supporting Information). It was found that high fluorescence quenching of MOFs occurs upon the incremental addition of NZF, while THI shows very low quenching effect (Figure 4a-d). Figure 4e shows the percentage of fluorescence quenching in terms of adding a certain amount of different antibiotics at room temperature. Obviously, NZF and NFT give rise to the highest quenching efficiencies of 92 and 91% for BUT-12, and 95 and 94% for BUT-13, respectively. In addition, FZD, ODZ, RDZ, and DTZ also lead to relative high quenching efficiencies, whereas quenching efficiencies are low for the remaining antibiotics (Figure S10-21 in the Supporting Information). The quenching efficiencies of BUT-12 for these antibiotics follow the order of NZF > NFT > FZD > ODZ > DTZ > RDZ > MDZ > CAP > SAM > SDZ> PCL > THI, and that of BUT-13 is NZF > NFT > FZD > ODZ > DTZ > RDZ > CAP > SAM > MDZ > SDZ > PCL > THI. It should also be pointed out that the frameworks of the two MOFs are intact after the sensing experiments, as confirmed by PXRD (Figure S56 and 57 in the Supporting Information).

The fluorescent quenching efficiency can be quantitatively explained by the Stern-Volmer (SV) equation: $(I_o/I) = 1 + K_{sv}[Q]$, where K_{sv} is the quenching constant (M^{-1}), [Q] is the molar concentration of the analyte, I_o and I are the luminescence intensities before and after addition of the analyte, respectively. As indicated in Figure 4a-d (inset), S10-21 (inset), and S22 of the Supporting Information, the SV plots for NZF and NFT are nearly linear at low concentration ranges, but subsequently deviate from linearity and bend upwards at higher concentrations. Such phenomena of nonlinear SV plots might be due to self-absorption or an energy-transfer process.[15,73-77] Whereas, the other antibiotics gave linear SV plots. BUT-12 and -13 have the highest K_{sv} values of 1.1×10^5 and 7.5×10^4 M^{-1} towards NZF, and 3.8×10^4 and 6.0×10^4 M^{-1} towards NFT, respectively (Table S5 in the Supporting Information). Based on the K_{sv} values and the standard deviations (S_b) for three repeated fluorescent measurements of blank solutions, the detection limit ($3S_b/K_{sv}$) of BUT-12 and -13 towards NZF were calculated to be 58 and 90 ppb, respectively (Table S6 in the Supporting Information).

The selective detection of antibiotics in water system is highly desirable for practical application. Above results demonstrate that BUT-12 and -13 have high quenching efficiencies towards NFs, but very poor towards THI and PCL antibiotics. Motivated by these findings, we further checked the detection selectivity for NFs in the presence THI or PCL. In a control experiment, the fluorescence spectra of BUT-12 and -13 dispersed in water were initially recorded, respectively. To these systems, a saturated aqueous solution of THI was initially added so that high affinity binding sites would be accessible to THI and then followed by NFs (1 mM); the corresponding emissions were monitored (for detail, see the Experimental Section). As can be seen from Figure S23-28 in the Supporting Information, the emission intensity of the two MOFs only shows slightly changes in the presence of excess THI. Upon introducing NFs into the mixture of the MOFs and THI, the fluorescence was significantly quenched. This result reveals that the interference from THI can be neglected, convincing the high quenching selectivities of the two MOFs towards NFs. Similarly, the addition of PCL also showed negligible effect on the fluorescence intensity, whereas NFs can quench effectively the fluorescence of the MOFs in the presence of PCL in water (Figure S23-28 in the Supporting Information). These results can be easily visualized by plotting the percentage fluorescence intensity versus volume of antibiotic added, as shown in Figure 4f and g. Where, the stepwise decrease in fluorescence intensity clearly demonstrates the selectivity of BUT-12 and -13 towards NFs, even in the presence of a higher concentration of THI or PCL. These highly selective detections in water system in the presence of THI or PCL make BUT-12 and -13 reliable sensing materials for NFs.

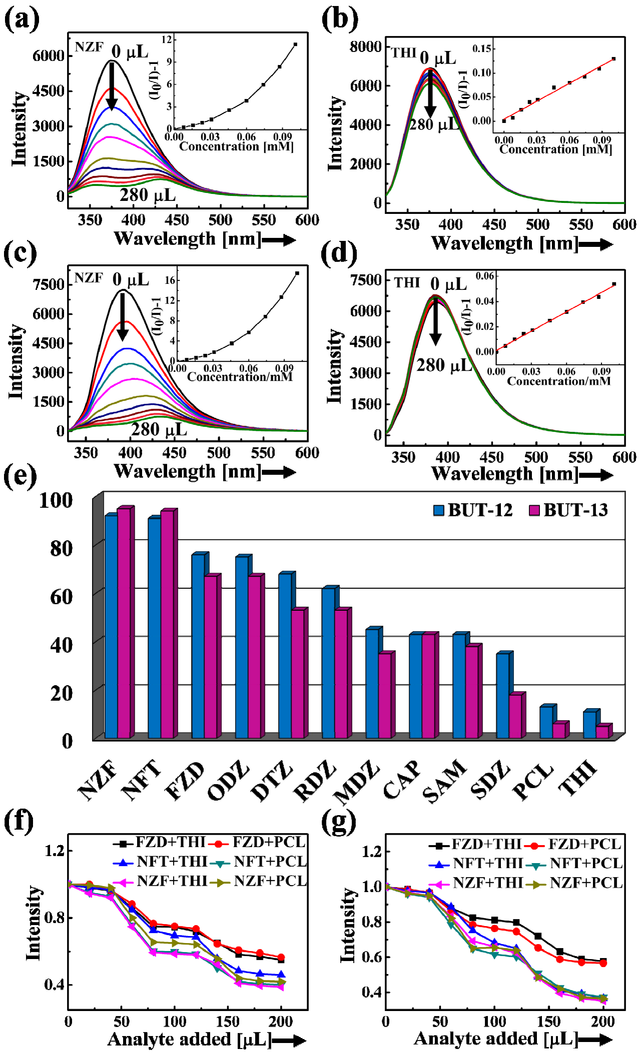

Figure 4. Effect on the emission spectra of (a, b) BUT-12 and (c, d) BUT-13 dispersed in water upon incremental addition of a selected antibiotic (1 mM, 20 μL addition each time; inset: Stern-Volmer plots of selected antibiotics); (e) fluorescence quenching of BUT-12 and -13 by different antibiotics at room temperature, and selective detection of NFs on (f) BUT-12 and (g) BUT-13 in the presence of THI or PCL in water.

On the other hand, until now a lot of MOFs have shown excellent performances for the detection of organic explosives and nitroaromatics based on their fluorescence quenching process.[18-20] However, most of them work in organic solvent systems, but not in water. High water stability of BUT-12 and -13 allows us to check their application in the detection of nitroaromatics in water. For comparison, some other aromatics and aliphatic nitro compounds were also tested. Here, eleven analytes including 2,4,6-trinitrophenol (TNP), 4-nitrophenol (4-NP), nitrobenzene (NB), 2,4-dinitrophenol (2,4-DNT), 2,6-dinitrophenol (2,6-DNT), benzoic acid (BC), chlorobenzene (CB), phenol (PHL), nitromethane (NM), methylbenzene (MB), and 2,3-dimethyl-2,3-dinitrobutane (DMNB) were checked (Figure S9 in the Supporting Information). As shown in Figure 5a-d and S29-40 of the Supporting Information, BUT-12 and -13 represent high quenching efficiencies of 98 and 96% and 97 and 95% towards TNP and 4-NP, respectively. Other nitroaromatics also give rise to high quenching efficiencies, but quenching efficiencies for non-nitroaromatics and aliphatic nitro compounds are low. The quenching efficiencies of BUT-12 follow the order of TNP > 4-NP > NB > 2,4-DNT > 2,6-DNT > BC > CB > PHL > NM > MB > DMNB, and that of BUT-13 is TNP > 4-NP > NB > 2,4-DNT > 2,6-DNT > DMNB > PHL > NM > BC > MB > CB (Figure 5e). The frameworks of the two MOFs are also intact after these detection experiments as confirmed by PXRD (Figure S56 and 57 in the Supporting Information).

Similar to those in detecting antibiotics, the SV plots of TNP and 4-NP are also nearly linear at low concentration ranges, then subsequently deviate from linearity and bend upwards at higher concentration ranges (Figure 5a-d inset, S29-40 inset, and S41 in the Supporting Information). Linear SV plots were observed for all the other analytes over a wide concentration range (Figure S41 in the Supporting Information). Both BUT-12 and -13 show the highest K_{sv} values of 3.1×10^5 and 5.1×10^5 M^{-1} for TNP, respectively. The detection limits of BUT-12 and -13 towards TNP are estimated to be 23 and 10 ppb, respectively (Table S6 in the Supporting Information). It should be pointed out that most of published works in the detection of nitroaromatics with MOFs are based on the checks in organic solvents such as CH_3OH, C_2H_5OH, DMF, and CH_3CN. Only UiO-67@N showed a good detection ability towards TNP in water. The K_{sv} for TNP in UiO-67@N was 2.9×10^4 M^{-1}, far smaller than those of BUT-12 and -13.[15] In addition, the K_{sv} values for TNP in the two MOFs are also larger than most traditionally used organic polymer sensing materials, demonstrating a super-quenching ability of them (Table S8 in the Supporting Information). The K_{sv} values calculated for other nitroaromatics are smaller than that of TNP (Table S5 in the Supporting Information). Furthermore, the selective fluorescence quenching of BUT-12 and -13 towards some nitroaromatics in the presence MB or CB were also studied (Figure S42-47 in the Supporting Information). As shown in Figure 5f and g, the stepwise decrease in fluorescence intensity clearly demonstrates the unprecedented selectivity of BUT-12 and -13 towards TNP, 4-NP, and NB, even in the presence of MB or CB with a high concentration.

In order to better understand the fluorescence quenching effect of BUT-12 and -13 towards NFs and nitroaromatics, the quenching mechanism was proposed. Simply, MOFs can be regarded as large "molecules" and the valence-band (VB) and conduction-band (CB) energy levels can be described in a mode similar to that used for molecular orbitals (MOs).[15,73-77] The CB of a MOF lies at higher energy level than the lowest unoccupied molecular orbitals (LUMOs) of an analyte, which leads to a driving force for the electron transfer from the MOF to the analyte, thus resulting in the fluorescence quenching. Shapes and relative orbital energies of the highest occupied molecular orbitals (HOMOs) and LUMOs of the analytes were herein calculated by DFT (Figure S58, 59 and Table S7 in the Supporting Information). These LUMO energy levels, which are arranged in a descending energy order, are expected to represent how easily an electron can be transferred to the electron-deficient analyte in the fluorescence quenching process. It was found that the LUMO energies are in good agreement with the maximum quenching efficiency observed for TNP, but the order of observed quenching efficiency is not fully in accordance with the LUMO energies of antibiotics and other nitroaromatics. These results indicate that the photo-induced electron transfer is not the only mechanism for the fluorescence quenching observed in these systems.

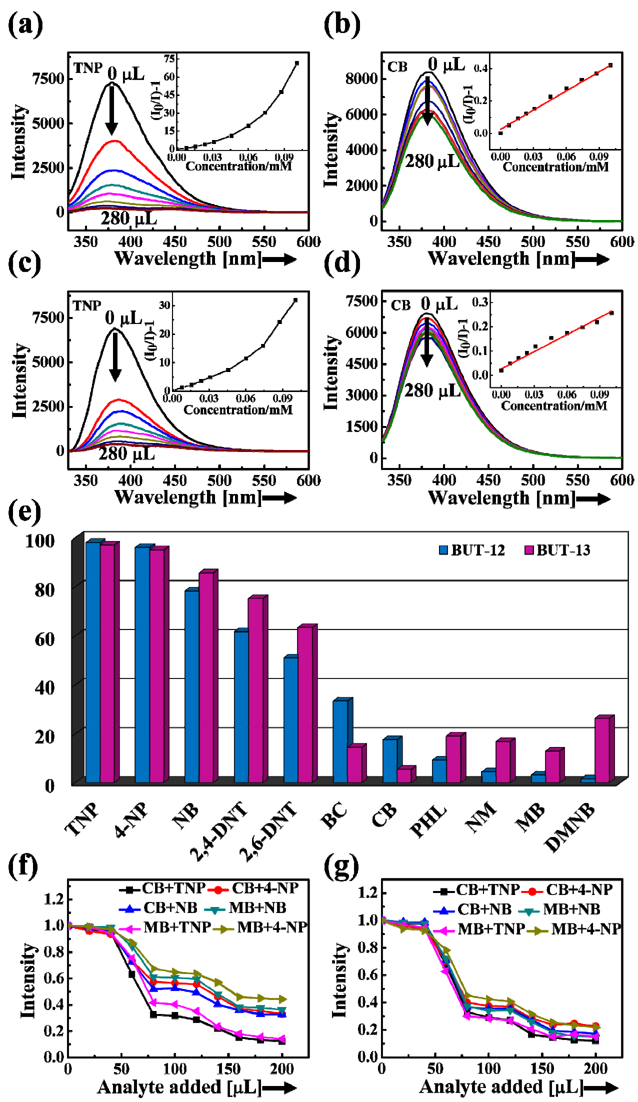

Figure 5. Effect on the emission spectra of (a, b) BUT-12 and (c, d) BUT-13 dispersed in water upon incremental addition of a selected analyte (1 mM, 20 μL addition each time; inset: SV plots of selected analyte); (e) fluorescence quenching of BUT-12 and -13 by different analytes at room temperature; and the selective detection of TNP, 4-NP or NB on (f) BUT-12 and (g) BUT-13 in the presence of CB or MB in water.

Another reason for the quenching might be the resonance energy transfer.[15,73,74] The nonlinearity of the SV plots for NZF, NFT, TNP, and 4-NP discussed above indeed suggests that such an energy transfer should exist in the fluorescence quenching processes. As we know, when the absorption band of the analyte has an effective overlap with the emission band of the MOF, the resonance energy can transfer from the MOF to the analyte, therefore the fluorescence quenching happening. The probability of resonance energy transfer thus depends upon the extent of spectral overlap between the absorption band of the analyte and the emission band of the MOF. As shown in the UV-vis absorption spectra of the analytes and the two MOFs (Figure S60 and 61 in the Supporting Information), the absorption band of NZF has the greatest degree of overlapping with the emission spectra of BUT-12 and -13, followed by NFT, FZD, ODZ, DTZ, MDZ, RDZ, SAM, CAP, SDZ, PCL, and THI. For nitroaromatics, TNP has the greatest overlap, followed by 4-NP, NB, 2,4-DNT, 2,6-DNT, NM, THL, DMNB, CB, MB, and BC. Clearly, the extents of the overlap are highly consistent with the quenching efficiencies for both antibiotics and nitroaromatics as discussed above. As a result, the co-existence of electron transfer and resonance energy transfer makes NFs and nitroaromatics show higher photo-luminescence quenching effect compared with other checked analytes.

The existence of energy transfer was also supported by the preferential quenching of the 374 nm peak over 430 nm in BUT-12, and 390 nm peak over 440 nm in BUT-13 (Figure 4a, c, 5a and c). The peaks at 374 nm of BUT-12 and 390 nm of BUT-13 have large spectral overlaps with the absorption spectra of NFs and nitroaromatics, so that the efficient quenching of the two peaks occurs, respectively, thereby giving higher quenching response. Whereas, the peaks at 430 nm of BUT-12 and 440 nm of BUT-13 have less overlap with the absorption spectra of them, thus the quenching occurs only based on an electron transfer mechanism, and a small quenching response towards other antibiotics and non-nitroaromatics were observed. These results also imply that the energy transfer is predominant over the electron transfer in the fluorescence quenching of the two MOFs by these antibiotics and nitroaromatics. For other analytes, the quenching occurs only by an electron transfer process. In addition, since the energy transfer is a long-range process, the emission quenching by NFs and nitroaromatics are carried over the surrounding fluorophores, thus amplifying the quenching response of BUT-12 and -13. While the electron transfer is a short-range process, the emission quenching by other analytes is limited to the fluorophore that has direct interaction with the analytes. Thus, BUT-12 and -13 respond more selectively towards NFs and nitroaromatics than other analytes. It should also be pointed out that BUT-12 and -13 can be recovered and regenerated by the centrifugation of the solution after use and washing with acetone several times. The quenching efficiencies up to 6 cycles are basically unchanged, demonstrating good recyclability and stability for these detection applications (Figure S62 and 63 in the Supporting Information).

Adsorption of antibiotics and nitroaromatics

Besides detection, the removal of antibiotics and nitroaromatics from wastewater are also important in water treatment. Reported results have shown that MOFs can be used as good adsorbents for the removal of organic contaminants from water.[23] However, to the best of our knowledge, the relevant studies on antibiotics and nitroaromatics are still scarce up to now. Thus we checked the adsorption performances of BUT-12 and -13 for some selected antibiotics (NFs, NMs, SAM, and CAP) and nitroaromatics (TNP, 4-NP, 2,4-DNT, 2,6-DNT, and NB). Freshly prepared BUT-12 and -13 were activated to remove guest molecules accommodated in their pores and then immersed in water solutions of these antibiotics and nitroaromatics at room temperature. The uptakes of these analytes in BUT-12 and -13 were determined by using UV-Vis spectroscopy. As shown in Figure 6a-d and S64-77 in the Supporting Information, BUT-12 represents large adsorption rates towards NZF and NFT antibiotics, and TNP, 4-NP, 2,4-DNT, and 2,6-DNT nitroaromatics; while BUT-13 can quickly adsorb NZF, NFT, ODZ, SAM, and CAP antibiotics, and TNP, 4-NP, 2,4-DNT, 2,6-DNT, and NB nitroaromatics. Different adsorption behaviors of BUT-12 and -13 should be related with their different pore sizes.

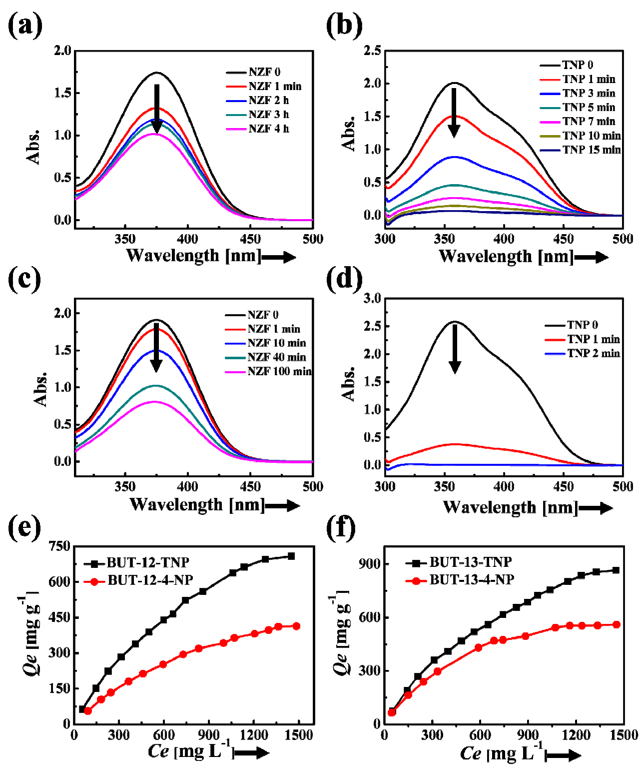

Figure 6. Adsorptions of NZF (a) and TNP (b) in BUT-12, and NZF (c) and TNP (d) in BUT-13, tracked by UV-vis spectra change with respect to time; and adsorption isotherms of TNP and 4-NP in BUT-12 (e) and BUT-13 (f) (adsorption conditions: at 298 K, 50 mL of solution, 15 mg of MOFs, contact time of 4 h).

It should be pointed out that, up to now, few works have been reported for antibiotic removal in water with the adsorption method. For comparison, we also carried out similar adsorption experiments of NZF and NFT for zeolites (5A, 3A, 13X, and Na-LSX) and mesoporous SiO_2 (SBA-15) in water. Before adsorption experiments, all adsorbents were activated at 100 °C under vacuum for 10 h. As shown in Figure S78-82 of the Supporting Information, zeolites 5A, 3A, 13X, Na-LSX, and SBA-15 show trace adsorption towards the two antibiotics. The hydrophilic nature and/or unmatched pore size of these materials are believed to be the main reason of the observed low uptakes. The sizes of NZF and NFT are of 9.34 × 2.25 and 8.91 × 3.52 Å, respectively (Figure S9, and Table S4 in the Supporting Information), implying that they should be able to diffuse into the pores of 5A, 13X (*ca.* 8 Å), and Na-LSX (*ca.* 10 Å) zeolites. However, the hydrophilic nature of the zeolites makes water molecules preferentially occupy their pores during the adsorption processes, thus limiting the access of the antibiotics. The interactions between the antibiotic molecules and SBA-15 are probably relatively weak because of its mesoporous nature (~60 Å), thus resulting in low uptakes. Additionally, SBA-15 is also moderately hydrophilic; the competitive adsorption of water may further lead to its low adsorption towards antibiotics. We thus propose that the suitable pore size and hydrophobic pore surface of a material might play key roles in the adsorption of these antibiotic molecules from water. The presence of methyl groups in the ligands of BUT-12 and -13 can increase the hydrophobicity of the two MOFs, which weakens their interactions with water molecules thus increasing their adsorption ability for antibiotics and nitroaromatics. The high contact angles of water (138.7 and 118.3°) suggest the hydrophobic property of BUT-12 and -13 (Figure S83 in the Supporting Information). Besides, water adsorption isotherms for BUT-12 and-13 were recorded at room temperature (Figure S84 in the Supporting Information). It was found that the two MOFs have high water uptakes of 540 and 615 $cm^3 g^{-1}$ at P/P_o = 0.86, respectively, which is in accordance with their high porosity. However, the water adsorption isotherms are stepwise with hysteresis loops and low uptakes at lower pressure ranges (below P/P_o = 0.27 for BUT-12, and P/P_o = 0.38 for BUT-13) followed by a steep rise of uptake at higher pressures. Compared with the total water uptakes, at low pressure ranges the uptakes (100.0 $cm^3 g^{-1}$ at P/P_o = 0.27 for BUT-12 and 92.7 $cm^3 g^{-1}$ at P/P_o = 0.38 for BUT-13) are relatively low (18.5 and 15.1% of the total uptakes, respectively), which indicates that pore surfaces of the two MOFs are dominatively hydrophobic notwithstanding there are also small portion of hydrophilic adsorption sites.[54] This is consistent with the single crystal structures of the two MOFs, which show that their pore walls mostly consists of backbone of organic linkers with hydrophobic methyl groups. The O/OH groups in Zr_6 clusters and coordinated carboxylate O atoms in ligands should be responsible to the small portion of hydrophilic adsorption sites on their pore surface.

For nitroaromatics, particularly, TNP and 4-NP can be completely adsorbed within 15 and 100 min in BUT-12, and within 2 and 40 min in BUT-13, respectively (Figure 6b and d). The faster adsorption kinetics in BUT-13 than that in BUT-12 can be attributed to the larger pore size of the former than that of the latter. With these results in mind, we further explored the adsorption isotherms of TNP and

4-NP in BUT-12 and -13 at 298 K. As shown in Figure 6e and f, the maximum adsorption amounts of TNP and 4-NP in BUT-12 are 708 and 414 mg/g, and those in BUT-13 are 865 and 560 mg/g, respectively. These values are comparable and/or even higher than those in other porous materials reported so far (Table S8 in the Supporting Information). In addition, the results of FT-IR measurements also confirm that TNP and 4-NP molecules are indeed adsorbed into the pores of the two MOFs (Figure S85 and 86 in the Supporting Information). The superior performances of the two MOFs in TNP and 4-NP adsorptions could be ascribed to their large specific surface areas, suitable pore size, as well as the distributing OH groups on pore surfaces, which endow the MOF strong interactions with the adsorbates. Moreover, Langmuir [78] and Freundlich [79] models were used to fit and examine above adsorption isotherms, respectively. The related parameters are given in Table S9, as well as the details in Figure S87-90 in the Supporting Information. Obviously, the data are well fitted by the Langmuir model, indicating a homogeneous and monolayer adsorption occurring in BUT-12 and -13 with a finite number of identical sites. Thus, it is expected that with further increasing their surface areas, the number of adsorption sites will increase, which will accordingly enhance their adsorption capacities. In addition, as shown in Figure S91, the two MOFs almost regained their initial adsorption capacities over three repeated cycles, demonstrating their high stability and good reusability.

Overall, above results demonstrate that BUT-12 and -13 have high selective fluorescence quenching efficiencies and good adsorption abilities towards NZF, NFT, TNP, and 4-NP. The detection sensitivities of the two MOFs are believed to be related with the pre-concentration effect of these analytes. That is, during the detection process, when analytes are added into MOF-containing solutions, part of the analytes are firstly adsorbed by the MOFs, which makes the analytes contact with MOFs more sufficiently, thereby leading to an enhanced florescent response. To verify such a pre-concentration effect, solubility partition coefficients of TNP and 4-NP in water/MOFs system were calculated. The solubility partition coefficient is the ratio of concentrations of the quencher molecules within the MOFs and in the water.[17] Based on adsorption data, the concentrations of TNP and 4-NP in the supernatant are known and the concentration of them in the pores of BUT-12 and -13 were calculated based on the equation (4) (see the Experimental Section). Thus, the solubility partition coefficients can be calculated through “the concentrations of TNP or 4-NP in the pores of BUT-12 and -13 divide their concentrations in the supernatants, respectively”. It was found that the averaged solubility partition coefficients of TNP and 4-NP in BUT-12/water system are 6891 and 3635, and those of them in BUT-13/water system are of 6217 and 3648, respectively. The large solubility partition coefficients of TNP and 4-NP in water/MOFs solution show that, in these systems, TNP and 4-NP tend to preferentially access the pores of the MOFs, thus demonstrating the pre-concentration effect. On the other hand, as discussed above, the fluorescence of the two Zr-MOFs is mainly attributed to the emission of their ligands; it thus allows us to estimate the pre-concentration effect by comparing the quenching constants (K_{sv}) of the MOFs with those of their corresponding ligand acids. In this regard, if the K_{sv} value of a MOF is larger than that of its corresponding ligand acid, then we can say that the pores of the MOF indeed play an important role in the pre-concentration quenching. Fluorescence-quenching titration experiments of the ligand acids, H_3CTTA and H_3TTNA towards TNP and 4-NP were thus carried out under the same conditions, and their K_{sv} values were calculated (Figure S52-55 in the Supporting Information). It concluded that the K_{sv} values of H_3CTTA towards TNP and 4-NP are 2.1×10^4 and 1.4×10^4 M^{-1}, and those of H_3TTNA are 1.0×10^4 and 1.4×10^4 M^{-1}, respectively. These values are clearly far smaller than those of their corresponding MOFs, BUT-12 and -13 (Table S5 in the Supporting Information), implying the effect of the pre-concentration of analytes on the fluorescent quenching.

Conclusion

Two new chemically stable fluorescent Zr(IV)-based MOFs have been designed, synthesized, and used in the selective detection and removal of antibiotics and nitroaromatics in/from water, showing excellent performances. Guided by a topological design approach, two ligands were rationally designed and resulting MOFs represented an expected **the-a** topology, being first examples among Zr-MOFs. Besides, the introduced methyl groups into the ligands actually increased the steric hindrance to fix the position of terminal phenyl rings thus eliminating non-radiative relaxation pathways and increase the fluorescence property of resulting MOFs. The two MOFs showed excellent selective detection ability towards NZF and NFT antibiotics and TNP and 4-NP organic explosives over other partners based on their sensitive fluorescence quenching. The detection limits of BUT-12 towards NZF and TNP are estimated to be 58 and 23 ppb, and those of BUT-13 are 90 and 10 ppb, respectively. The high quenching efficiencies can be attributed to a combining effect from electron and energy transfers in the host-guest systems. Both MOFs show also good adsorption ability towards NZF, NFT, 4-NP, and TNP. Among them, the uptakes for 4-NP and TNP are comparable to those reported porous materials. Moreover, it was found that the adsorption process plays an important role in the pre-concentration of the analytes in the pores of the two MOFs, which makes the analytes contact with MOFs more sufficiently, thus enhancing the detection efficiency. Present study provides a new insight into the design of MOFs for the simultaneously detection and removal of contaminations in water. The resulting new MOF materials are potentially useful for the water treatment applications.

Experimental section

Materials and instruments

All general chemicals and solvents (AR grade) were commercially available and used as received. ^{1}H NMR spectra were measured on Bruker Avance 400 MHz with tetramethylsilane as the internal standard. FT-IR data were recorded on an SHIMADZU IR Affinity-1 instrument. Powder X-ray diffraction (PXRD) patterns were recorded on a BRUKER D8-Focus Bragg-Brentano X-ray Powder Diffractometer equipped with a Cu sealed tube (λ = 1.54178) at room temperature. Simulation of the PXRD spectra was carried out by the single-crystal data and diffraction-crystal module of the Mercury program available free of charge via internet at http://www.ccdc.cam.ac.uk/mercury/. Thermogravimetric analysis (TGA) data were obtained on a TGA-50 (SHIMADZU) thermogravimetric analyzer with a heating rate of 10 °C min^{-1} under air atmosphere. The contact angles towards water were measured on Dataphysics tp50. Gas adsorption isotherms were reported by a volumetric method using a Micromeritics ASAP2020 surface area and pore analyzer. Fluorescence spectra were recorded on an F-4600 FL Spectrophotometer equipped with a xenon lamp and quartz carrier at room temperature. UV/vis spectra were obtained with a UV-2600 spectrophotometer in the range of 250~800 nm at room temperature.

Synthesis

The ligand acids, 5'-(4-carboxyphenyl)-2',4',6'-trimethyl-[1,1':3',1''-terphenyl]-4,4''-dicarboxylic acid (H_3CTTA) and 6,6',6''-(2,4,6-trimethylbenzene-1,3,5-triyl)tris(2-napthoic acid) (H_3TTNA) were synthesized by following a previously reported procedures with some modifications.[80] The detailed description is provided in the Supporting Information.

[$Zr_6O_4(OH)_8(H_2O)_4(CTTA)_{8/3}$]·*S* (BUT-12·*S*) (*S* represents non-assignable solvent molecules): $ZrCl_4$ (48 mg, 0.2 mmol), H_3CTTA (40 mg, 0.08 mmol), and formic acid (8 mL) were ultrasonically dissolved in *N,N'*-dimethylformamide (DMF, 8 mL) in a 20 mL Pyrex vial. The vial was sealed and then heated at 120 °C for 48 h in an oven. After cooling to room temperature, the resulting colorless crystals were harvested by filtration and washed with DMF and acetone, and then dried in air (yielded 32 mg). For PXRD pattern of as-synthesized material, see Figure 3a; for TGA, and FT-IR, see Figure S3 and 4 of the Supporting Information, respectively.

[$Zr_6O_4(OH)_8(H_2O)_4(TTNA)_{8/3}$]·*S* (BUT-13·*S*) (*S* represents non-assignable solvent molecules): $ZrCl_4$ (48 mg, 0.2 mmol), H_3TTNA (40 mg, 0.06 mmol), and acetic acid (3.2 mL) were ultrasonically dissolved in 12 mL of DMF in a 20 mL Pyrex vial and sealed. The reaction system was then heated at 120 °C for 72 h in an oven. After cooling to room temperature, the resulting colorless crystals were collected by filtration and washed with DMF and acetone, and then dried in air (yielded 38 mg). For PXRD pattern of as-synthesized material, see Figure 3b; for TGA, and FT-IR, see Figure S3 and 4 of the Supporting Information, respectively.

Sample activation

As-synthesized samples were soaked in fresh DMF for 24 h, and the extract was discarded. Fresh acetone was subsequently added, and the samples were guest exchanged for 12 h. This procedure was again repeated three times. After decanting the acetone extract, the samples were dried under a dynamic vacuum (< 10^{-3} Torr) at room temperature for 1 h. Before adsorption measurement, the samples were further activated using the "outgas" function of the adsorption analyzer at 100 °C for 10 h.

Single-crystal X-ray diffraction

The diffraction data of BUT-12·*S* were collected in a Rigaku Supernova CCD diffractometer equipped with a mirror-monochromatic enhanced Cu-*K*α radiation (λ = 1.54184 Å) at 100 K. The dataset was corrected by empirical absorption correction using spherical harmonics, implemented in the SCALE3 ABSPACK scaling algorithm.[81] The structure was solved by direct methods and refined by full-matrix least-squares on F^2 with anisotropic displacement by using the SHELXTL software package.[82] Non-hydrogen atoms were refined with anisotropic displacement parameters during the final cycles. Hydrogen atoms of ligands were calculated in ideal positions with isotropic displacement parameters. Those in –OH/H_2O groups of the Zr(IV)-based clusters were not added, but were calculated into molecular formula of the crystal data. There is large solvent accessible pore volume in the structure of BUT-12, which is occupied by highly disordered solvent molecules. No satisfactory disorder model for these solvent molecules could be achieved, and therefore the SQUEEZE program implemented in PLATON was used to remove these electron densities of these disordered species.[69] Thus, all of electron densities from free solvent molecules have been "squeezed" out. The details of crystal data and structural refinement can be found in Tables S1 of the Supporting Information, and the provided CIF files.

Fluorescence measurements

Caution: *TNP and 2,4-DNT are highly explosive and should be handled carefully and in small amounts. In addition, TNP is also easy to form shock-sensitive compounds when meet with heavy metals.*

In a typical experimental setup, 2 mg of BUT-12 or -13 sample was weighed and finely grounded, and then added to a cuvette containing 2.5 mL of deionized water under stirring. The fluorescence upon excitation at 312 nm of BUT-12 and 324 nm of BUT-13 was measured in-situ after incremental addition of freshly prepared analyte solutions (1mM, 20 μL addition each time). The mixed solution was stirred at constant rate during experiment to maintain its homogeneity. All the experiments were performed in triplicate, and consistent results were reported.

Similarly, in a selective detection experiment, 2 mg finely grounded sample was added to a cuvette containing 2.5 mL of deionized water under stirring. Fluorescence of the obtained suspension was recorded. Then, saturated THI (or PCL, CB, and MB) and 1 mM NZF (or NFT, FZD, TNP, and 4-TN) solutions were alternatively introduced into the suspension in such a sequence: THI (20 ml), THI

(20 ml), NZF (20 ml), NZF (20 ml), THI (20 ml), THI (20 ml)..., the process was repeated till the total volume of added analytes reached 200 μL. After each addition, the fluorescence of the suspension was monitored.

Aqueous-phase adsorption

Freshly prepared BUT-12 or -13 sample (10 mg) was totally activated and then transferred into water solutions of different analytes with given concentrations in a vial, respectively. UV-vis spectra of the solutions were recorded to characterize the adsorption performances of BUT-12 and -13 along with the soaking time at 298 K. The adsorption isotherms of TNP and 4-NP were obtained by mixing 15 mg MOFs with 50 mL TNP or 4-NP solution of different concentrations from 100 to 1600 mg L^{-1} at a constant temperature of 298 K with stirring for 4 h. The amount of TNP or 4-NP adsorbed on the MOFs was calculated using the mass balance with Eq. 1:

$$Q_e = \frac{(C_o - C_e)V}{M} \qquad (1)$$

where Q_e (mg g^{-1}) is the equilibrium adsorbed amount; C_o and C_e (mg L^{-1}) are the initial and equilibrium concentrations of solution; V (L) is the volume of solution; M (g) is the mass of MOF. In order to assure the accuracy of measurements, all the experiments were repeated at least three times and the average values were reported. All materials were dried overnight under vacuum at 373 K before each repeated use. The resulting isotherms are fitted by Langmuir mode (Eq. 2):

$$\frac{C_e}{Q_e} = \frac{1}{K_L Q_m} + \frac{C_e}{Q_m} \qquad (2)$$

and Freundlich mode (Eq. 3):

$$\ln Q_e = \ln K_F + \frac{1}{n}\ln C_e \qquad (3)$$

where C_e (mg L^{-1}) is the equilibrium concentration of adsorbate; Q_e (mg L^{-1}) is the adsorbed amount at equilibrium; Q_m (mg L^{-1}) is the maximum monolayer adsorption capacity; K_L (L g mg L^{-1}) is the Langmuir constant related to the free energy of adsorption; K_F ((L mg^{-1})1/nmg g^{-1}) is the Freundlich adsorption constant, and 1/n is a measure of adsorption intensity ranging between 0 and 1. The concentrations of TNP and 4-NP in the pores of BUT-12 and -13 were calculated based on the following equation (4)

$$C_{MOF} = \frac{(C_0 - C_e)V_{solution}}{V_{MOF}} \qquad (4)$$

where C_{MOF} (mg L^{-1}) is the concentration of adsorbent in the pores of MOFs; C_o and C_e (mg L^{-1}) are the initial and equilibrium concentrations of the solution, respectively; $V_{solution}$ (L) is the volume of solution; V_{MOF} (m^3 g^{-1}) is the calculated total pore volume of the MOF.

Regeneration of adsorbents

The MOF adsorbents used in adsorption measurements were washed with acetone (by a proportion of 150 mL acetone per 15 mg MOFs) through soaking overnight under stirring at room temperature for 12 h. This procedure was repeated at least three times by using fresh acetone. After filtration, the wet products were dried under vacuum at 393 K for 2 h to remove the residual solvents. The regenerated MOFs were used again for the adsorption of TNP or 4-NP up to three cycles.

ASSOCIATED CONTENT

Supporting Information

Full details for the synthesis of H_3CTTA and H_3TTNA, structure refinement and construction, general characterizations, additional structural figures, DFT calculation, detection of antibiotics and nitroaromatics, adsorption towards selected antibiotics and nitroaromatics. This material is available free of charge via the Internet at http://pubs.acs.org.

AUTHOR INFORMATION

Corresponding Author

jrli@bjut.edu.cn

Notes

The authors declare no competing financial interest.

ACKNOWLEDGMENTS

We thank Dr. Hongliang Huang of Beijing University of Chemical Technology for his discussion in computational simulations and Prof. Daqiang Yuan of Fujian Institute of Research on the Structure of Matter for his help in structural analysis. This work was financially supported from the Natural Science Foundation of China (21322601, 21576006, 21271015) and the Program for New Century Excellent Talents in University of China (NCET-13-0647).

REFERENCES

(1) Kümmerer, K. *Chemosphere* **2009**, *75*, 417.

(2) Zhang, Q.-Q.; Ying, G.-G.; Pan, C.-G.; Liu, Y.-S.; Zhao, J.-L. *Environ. Sci. Technol.* **2015**, *49*, 6772.

(3) Blasco, C.; Corcia, A. D.; Picó, Y. *Food Chem.* **2009**, *116*, 1005.

(4) Benito-Peña, E.; Urraca, J. L.; Moreno-Bondi, M. C. *J. Pharm. Biomed. Anal.* **2009**, *49*, 289.

(5) Moreno-González, D.; Lara, F. J.; Jurgovská, N.; Gámiz-Gracia, L.; García-Campaña, A. M. *Anal. Chim. Acta* **2015**, *891*, 321.

(6) Håkansson, K.; Coorey, R. V.; Zubarev, R. A.; Talrose, V. L.; Håkansson, P. *J. Mass Spectrom.* **2000**, *35*, 337.

(7) Moros, J.; Laserna, J. J. *Anal. Chem.* **2011**, *83*, 6275.

(8) Tabrizchi, M.; ILbeigi, V. *J. Hazard. Mater.* **2010**, *176*, 692.

(9) Paul, T.; Miller, P. L.; Strathmann, T. J. *Environ. Sci. Technol.* **2007**, *41*, 4720.

(10) Li, D.; Yang, M.; Hu, J.; Zhang, Y.; Chang, H.; Jin, F. *Water Res.* **2008**, *42*, 307.

(11) González, O.; Sans, C.; Esplugas, S. *J. Hazard. Mater.* **2007**, *146*, 459.

(12) Hu, D.; Coats, J. R. *Environ. Toxicol. Chem.* **2007**, *26*, 884.

(13) Germain, M. E.; Knapp, M. J. *Chem. Soc. Rev.* **2009**, *38*, 2543.

(14) Ahmaruzzaman, M. *Adv. Colloid Interface Sci.* **2008**, *143*, 48.

(15) Nagarkar, S. S.; Desai, A. V.; Ghosh, S. K. *Chem. Commun.* **2014**, *50*, 8915.

(16) Lin, X.; Hong, Y.; Zhang, C.; Huang, R.; Wang, C.; Lin, W. *Chem. Commun.* **2015**, *51*, 16996.
(17) Wanderley, M. M.; Wang, C.; Wu, C.-D.; Lin, W. *J. Am. Chem. Soc.* **2012**, *134*, 9050.
(18) Cui, Y.; Yue, Y.; Qian, G.; Chen, B. *Chem. Rev.* **2012**, *112*, 1126.
(19) Kreno, L. E.; Leong, K.; Farha, O. K.; Allendorf, M.; Van Duyne, R. P.; Hupp, J. T. *Chem. Rev.* **2012**, *112*, 1105.
(20) Hu, Z.; Deibert, B. J.; Li, J. *Chem. Soc. Rev.* **2014**, *43*, 5815.
(21) Guo, Y.; Feng, X.; Han, T.; Wang, S.; Lin, Z.; Dong, Y.; Wang, B. *J. Am. Chem. Soc.* **2014**, *136*, 15485.
(22) Ye, J.-W.; Zhou, H.-L.; Liu, S.-Y.; Cheng, X.-N.; Lin, R.-B.; Qi, X.-L.; Zhang, J.-P.; Chen, X.-M. *Chem. Mater.* **2015**, *27*, 8255.
(23) Van de Voorde, B.; Bueken, B.; Denayer, J.; De Vos, D. *Chem. Soc. Rev.* **2014**, *43*, 5766.
(24) Li, B.; Wen, H.-M.; Wang, H.; Wu, H.; Tyagi, M.; Yildirim, T.; Zhou, W.; Chen, B. *J. Am. Chem. Soc.* **2014**, *136*, 6207.
(25) Jiang, X.; Liu, Y.; Wu, P.; Wang, L.; Wang, Q.; Zhu, G.; Li, X.-L.; Wang, J. *RSC Adv.* **2014**, *4*, 47357.
(26) Jhung, S. H.; Lee, J.-H.; Yoon, J. W.; Serre, C.; Férey, G.; Chang, J.-S. *Adv. Mater.* **2007**, *19*, 121.
(27) Tong, M.; Liu, D.; Yang, Q.; Devautour-Vinot, S.; Maurin, G.; Zhong, C. *J. Mater. Chem. A* **2013**, *1*, 8534.
(28) Cychosz, K. A.; Matzger, A. J. *Langmuir* **2010**, *26*, 17198.
(29) Zhou, M.; Wu, Y.-N.; Qiao, J.; Zhang, J.; McDonald, A.; Li, G.; Li, F. *J. Colloid Interface Sci.* **2013**, *405*, 157.
(30) Jung, B. K.; Hasan, Z.; Jhung, S. H. *Chem. Eng. J.* **2013**, *234*, 99.
(31) Maes, M.; Schouteden, S.; Alaerts, L.; Depla, D.; De Vos, D. E. *Phys. Chem. Chem. Phys.* **2011**, *13*, 5587.
(32) Liu, B.; Yang, F.; Zou, Y.; Peng, Y. *J. Chem. Eng. Data* **2014**, *59*, 1476.
(33) Patil, D. V.; Rallapalli, P. B. S.; Dangi, G. P.; Tayade, R. J.; Somani, R. S.; Bajaj, H. C. *Ind. Eng. Chem. Res.* **2011**, *50*, 10516.
(34) Hasan, Z.; Jhung, S. H. *J. Hazard. Mater.* **2015**, *283*, 329.
(35) Dias, E. M.; Petit, C. *J. Mater. Chem. A* **2015**, *3*, 22484.
(36) Canivet, J.; Fateeva, A.; Guo, Y.; Coasne, B.; Farrusseng, D. *Chem. Soc. Rev.* **2014**, *43*, 5594.
(37) Burtch, N. C.; Jasuja, H.; Walton, K. S. *Chem. Rev.* **2014**, *114*, 10575.
(38) Wang, X.; Gao, W.-Y.; Luan, J.; Wojtas, L.; Ma, S. *Chem. Commun.* **2016**, *52*, 1971.
(39) Nguyen, J. G.; Cohen, S. M. *J. Am. Chem. Soc.* **2010**, *132*, 4560.
(40) Yang, C.; Kaipa, U.; Mather, Q. Z.; Wang, X.; Nesterov, V.; Venero, A. F.; Omary, M. A. *J. Am. Chem. Soc.* **2011**, *133*, 18094.
(41) Serre, C. *Angew. Chem. Int. Ed.* **2012**, *51*, 6048.
(42) Jasuja, H.; Huang, Y.-G.; Walton, K. S. *Langmuir* **2012**, *28*, 16874.
(43) Padial, N. M.; Quartapelle Procopio, E.; Montoro, C.; López, E.; Oltra, J. E.; Colombo, V.; Maspero, A.; Masciocchi, N.; Galli, S.; Senkovska, I.; Kaskel, S.; Barea, E.; Navarro, J. A. R. *Angew. Chem. Int. Ed.* **2013**, *52*, 8290.
(44) He, C.-T.; Jiang, L.; Ye, Z.-M.; Krishna, R.; Zhong, Z.-S.; Liao, P.-Q.; Xu, J.; Ouyang, G.; Zhang, J.-P.; Chen, X.-M. *J. Am. Chem. Soc.* **2015**, *137*, 7217.
(45) Férey, G.; Mellot-Draznieks, C.; Serre, C.; Millange, F.; Dutour, J.; Surblé, S.; Margiolaki, I. *Science* **2005**, *309*, 2040.
(46) Feng, D.; Wang, K.; Wei, Z.; Chen, Y.-P.; Simon, C. M.; Arvapally, R. K.; Martin, R. L.; Bosch, M.; Liu, T.-F.; Fordham, S.; Yuan, D.; Omary, M. A.; Haranczyk, M.; Smit, B.; Zhou, H.-C. *Nat. Comms.* **2014**, *5*, 5723.
(47) Cavka, J. H.; Jakobsen, S.; Olsbye, U.; Guillou, N.; Lamberti, C.; Bordiga, S.; Lillerud, K. P. *J. Am. Chem. Soc.* **2008**, *130*, 13850.
(48) Yang, S.; Sun, J.; Ramirez-Cuesta, A. J.; Callear, S. K.; David, W. I. F.; Anderson, D. P.; Newby, R.; Blake, A. J.; Parker, J. E.; Tang, C. C.; Schröder, M. *Nature. Chem.* **2012**, *4*, 887.
(49) Schaate, A.; Roy, P.; Godt, A.; Lippke, J.; Waltz, F.; Wiebcke, M.; Behrens, P. *Chem. Eur. J.* **2011**, *17*, 6643.
(50) Bai, Y.; Dou, Y.; Xie, L.-H.; Rutledge, W.; Li, J.-R.; Zhou, H.-C. *Chem. Soc. Rev.* **2016**, *45*, 2327.
(51) Delgado-Friedrichs, O.; O'Keeffe, M.; Yaghi, O. M. *Acta Crystallogr., Sect. A: Found. Crystallogr.* **2006**, *62*, 350.
(52) Zhang, M.; Chen, Y.-P.; Bosch, M.; Gentle III, T.; Wang, K.; Feng, D.; Wang, Z. U.; Zhou, H.-C. *Angew. Chem. Int. Ed.* **2014**, *53*, 815.
(53) Liu, T.-F.; Feng, D.; Chen, Y.-P.; Zou, L.; Bosch, M.; Yuan, S.; Wei, Z.; Fordham, S.; Wang, K.; Zhou, H.-C. *J. Am. Chem. Soc.* **2015**, *137*, 413.
(54) Furukawa, H.; Gándara, F.; Zhang, Y.-B.; Jiang, J.; Queen, W. L.; Hudson, M. R.; Yaghi, O. M. *J. Am. Chem. Soc.* **2014**, *136*, 4369.
(55) Bon, V.; Senkovska, I.; Baburin, I. A.; Kaskel, S. *Cryst. Growth Des.* **2013**, *13*, 1231.
(56) Mondloch, J. E.; Bury, W.; Fairen-Jimenez, D.; Kwon, S.; DeMarco, E. J.; Weston, M. H.; Sarjeant, A. A.; Nguyen, S. T.; Stair, P. C.; Snurr, R. Q.; Farha, O. K.; Hupp, J. T. *J. Am. Chem. Soc.* **2013**, *135*, 10294.
(57) Feng, D.; Gu, Z.-Y.; Li, J.-R.; Jiang, H.-L.; Wei, Z.; Zhou, H.-C. *Angew. Chem. Int. Ed.* **2012**, *51*, 10307.
(58) Bon, V.; Senkovskyy, V.; Senkovska, I.; Kaskel, S. *Chem. Commun.* **2012**, *48*, 8407.
(59) Wang, S.; Wang, J.; Cheng, W.; Yang, X.; Zhang, Z.; Xu, Y.; Liu, H.; Wu, Y.; Fang, M. *Dalton Trans.* **2015**, *44*, 8049.
(60) Feng, D.; Wang, K.; Su, J.; Liu, T.-F.; Park, J.; Wei, Z.; Bosch, M.; Yakovenko, A.; Zou, X.; Zhou, H.-C. *Angew. Chem. Int. Ed.* **2015**, *54*, 149.
(61) Wang, R.; Wang, Z.; Xu, Y.; Dai, F.; Zhang, L.; Sun, D. *Inorg. Chem.* **2014**, *53*, 7086.
(62) Wei, Z.; Gu, Z.-Y.; Arvapally, R. K.; Chen, Y.-P.; McDougald, R. N.; Ivy, J. F.; Yakovenko, A. A.; Feng, D.; Omary, M. A.; Zhou, H.-C. *J. Am. Chem. Soc.* **2014**, *136*, 8269.
(63) Shustova, N. B.; Ong, T.-C.; Cozzolino, A. F.; Michaelis, V. K.; Griffin, R. G.; Dincă, M. *J. Am. Chem. Soc.* **2012**, *134*, 15061.
(64) Hu, Z.; Lustig, W. P.; Zhang, J.; Zheng, C.; Wang, H.; Teat, S. J.; Gong, Q.; Rudd, N. D.; Li, J. *J. Am. Chem. Soc.* **2015**, *137*, 16209.
(65) Zhang, L.-J.; Han, C.-Y.; Dang, Q.-Q.; Wang, Y.-H.; Zhang, X.-M. *RSC Adv.* **2015**, *5*, 24293.
(66) Dincã, M.; Dailly, A.; Liu, Y.; Brown, C. M.; Neumann, D. A.; Long, J. R. *J. Am. Chem. Soc.* **2006**, *128*, 16876.
(67) Colombo, V.; Galli, S.; Choi, H. J.; Han, G. D.; Maspero, A.; Palmisano, G.; Masciocchi, N.; Long, J. R. *Chem. Sci.* **2011**, *2*, 1311.
(68) Gomez-Gualdron, D. A.; Gutov, O. V.; Krungleviciute, V.; Borah, B.; Mondloch, J. E.; Hupp, J. T.; Yildirim, T.; Farha, O. K.; Snurr, R. Q. *Chem. Mater.* **2014**, *26*, 5632.
(69) Spek, A. L. *J. Appl. Cryst.* **2003**, *36*, 7.
(70) Lv, X.-L.; Tong, M.; Huang, H.; Wang, B.; Gan, L.; Yang, Q.; Zhong, C.; Li, J.-R. *J. Solid State Chem.***2015**, *223*, 104.
(71) Wang, K.; Huang, H.; Xue, W.; Liu, D.; Zhao, X.; Xiao, Y.; Li, Z.; Yang, Q.; Wang, L.; Zhong, C. *CrystEngComm* **2015**, *17*, 3586.
(72) Kang, I. J.; Khan, N. A.; Haque, E.; Jhung, S. H. *Chem. Eur. J.* **2011**, *17*, 6437.
(73) Nagarkar, S. S.; Joarder, B.; Chaudhari, A. K.; Mukherjee, S.; Ghosh, S. K. *Angew. Chem. Int. Ed.* **2013**, *52*, 2881.

(74) Shi, Z.-Q.; Guo, Z.-J.; Zheng, H.-G. *Chem. Commun.* **2015**, *51*, 8300.
(75) Sohn, H.; Sailor, M. J.; Magde, D.; Trogler, W. C. *J. Am. Chem. Soc.* **2003**, *125*, 3821.
(76) Zhang, Q.; Geng, A.; Zhang, H.; Hu, F.; Lu, Z.-H.; Sun, D.; Wei, X.; Ma, C. *Chem. Eur. J.* **2014**, *20*, 4885.
(77) Pramanik, S.; Zheng, C.; Zhang, X.; Emge, T. J.; Li, J. *J. Am. Chem. Soc.* **2011**, *133*, 4153.
(78) Galán, J.; Rodríguez, A.; Gómez, J. M.; Allen, S. J.; Walker, G. M. *Chem. Eng. J.* **2013**, *219*, 62.
(79) Wang, L.; Huang, Z.; Zhang, M.; Chai, B. *Chem. Eng. J.* **2012**, *189-190*, 168.
(80) Zhao, X.; Dou, J.; Sun, D.; Cui, P.; Sun, D.; Wu, Q. *Dalton Trans.* **2012**, *41*, 1928.
(81) SCALE3 ABSPACK scaling algorithm. CrysAlis RED, Oxford Diffraction Ltd., Version 1.171.32.38.
(82) Sheldrick, G. M. SHELXTL 2008/4, Structure determination software suite; Bruker AXS Inc.: Madison, WI.

TOC